Infrared reflectivity and lattice fundamentals in anatase TiO_2

R. J. Gonzalez* and R. Zallen
Department of Physics, Virginia Tech, Blacksburg, Virginia 24061

H. Berger
Institut de Physique Appliquee, Ecole Polytechnique Federale Lausanne, Switzerland CH-1015

(Received 9 July 1996; revised manuscript received 21 October 1996)

Polarization-dependent far-infrared reflectivity measurements were carried out on single crystals of anatase TiO_2. The results were analyzed to yield the dielectric dispersion properties of anatase in the lattice fundamentals regime. The frequencies (in cm^{-1}) of the transverse optical (TO) and longitudinal optical (LO) zone-center phonons were determined to be 367(755) for the TO (LO) of the A_{2u} mode, 262(366) and 435(876) for the E_u modes. The large TO-LO splittings were used to estimate effective charges. [S0163-1829(97)02009-2]

I. INTRODUCTION

The crystal forms of titanium dioxide (titania) are rutile, anatase, and brookite. They are wide-bandgap semiconductors, transparent in the visible, with high refractive indices. Rutile is the stable phase at high temperature and is by far the most-studied and best-understood phase. Because large single crystals of rutile have long been long available, the lattice dynamics of rutile TiO_2 in the lattice-fundamentals regime has been studied by polarization-dependent far-infrared reflectivity measurements[1,2] and by neutron-scattering measurements as well.[3] To our knowledge, no similar work has yet been reported for anatase TiO_2, although there have been studies of the Raman-active lattice fundamentals.[4] The near-bandgap optical absorption edge of anatase has recently been measured.[5]

In this paper, we present the results of far-infrared reflectivity measurements on anatase single crystals. The polarization-dependent single-crystal results are analyzed to yield the zone-center transverse-optical (TO) and longitudinal-optical (LO) phonon frequencies, effective charges, and polariton dispersion curves of anatase.

II. EXPERIMENT

Anatase crystals were grown by chemical transport reactions.[6] As-grown single crystals were up to 5 mm in size, with an octahedral shape limited by (101) natural faces. Two crystals were used in this study. There were cut and polished; one to yield a surface containing the tetragonal c axis, the other to yield a surface perpendicular to the c axis. Alumina powder was used for polishing, the final grit size being 0.1 μm. The area of the optical surface was about 8 mm^2 for the parallel-to-c surface and about 9 mm^2 for the perpendicular-to-c surface.

The infrared measurements were performed with a BOMEM DA-3 FTIR spectrometer. A pyroelectric detector was used to cover the wave-number region from 50 to 700 cm^{-1}; a HgCdTe detector was used from 600 to 5000 cm^{-1}. Spectra were collected with a 1-cm^{-1} resolution. At least 400 interferometer sweeps were added for each spectrum. For measurements with light polarized parallel to the crystal c axis, a wire-grid polarizer was used. (The low-frequency cutoff, determined by the polarizer substrate, was 200 cm^{-1}.) Reflectivity was measured at an angle of incidence of 11°, and was determined by comparison to an aluminum mirror standard.

III. INFRARED-ACTIVE MODES OF ANATASE

Anatase is tetragonal, with two TiO_2 formula units (six atoms) per primitive cell. The space group is D_{4h}^{19} ($I4/amd$), number 141 in the standard listing. The structure is shown on the left side of Fig. 1. The c-axis is vertical, small circles denote Ti atoms, large circles denote O atoms. Oxygen atoms labeled with the same number are equivalent. The octahedral coordination of the titanium atoms is seen to be significantly distorted.

The 18-dimensional reducible representation generated by the atomic displacements contains the zone-center ($k=0$) modes: 3 acoustic modes and 15 optical modes. The irreducible representations corresponding to the 15 optical modes

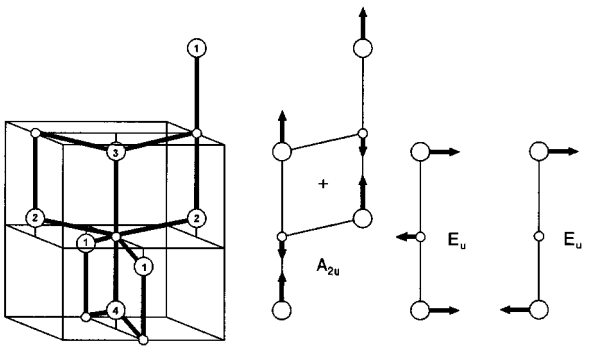

FIG. 1. The structure of the anatase primitive cell is shown at the left. The c axis is vertical, small circles denote Ti atoms, large circles denote O atoms. Oxygen atoms labeled with the same number are equivalent. The center figure shows (+) the position of the inversion center and the vibrational eigenvector for the A_{2u} mode. Symmetry coordinates for the E_u modes are shown at the right.

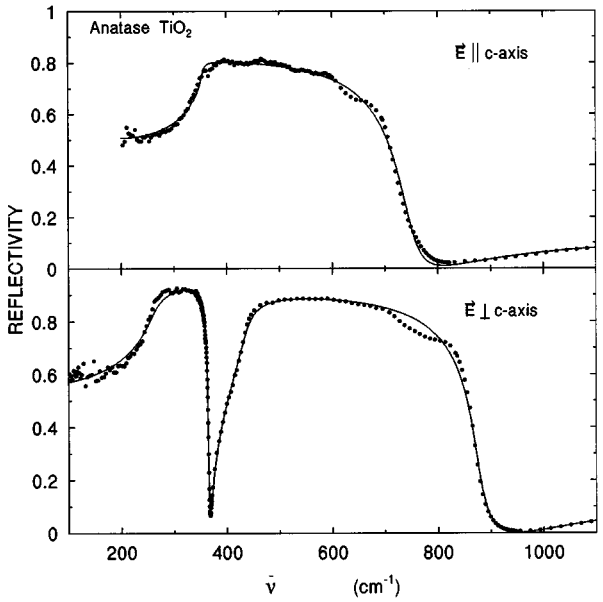

FIG. 2. The polarization-dependent far-infrared reflectivity of single-crystal anatase. The $E\|c$ results, obtained for a surface containing the c axis, required the use of a polarizer which cut off below 200 cm^{-1}. The $E\perp c$ results, obtained for a surface normal to the c axis, required no polarizer and extended down to 50 cm^{-1}. (The 50–100 cm^{-1} range, not shown, contained no discernible structure.) The continuous curves included in this figure are fits based on the factorized form of the dielectric function [Eq. (1)].

are[4] $1A_{1g}+1A_{2u}+2B_{1g}+1B_{2u}+3E_g+2E_u$. Three modes are infrared active, the A_{2u} mode and the two E_u modes. (The B_{2u} mode is silent.) The A_{2u} mode is active for light polarized parallel to the c axis ($E\|c$); the E_u modes are active for light polarized perpendicular to the c axis ($E\perp c$). The vibrational eigenvector for the A_{2u} is symmetry-determined; it is shown in Fig. 1. Symmetry coordinates for the E_u modes are also shown. The actual E_u eigenvectors are mutually orthogonal combinations of these.

IV. POLARIZATION-DEPENDENT REFLECTIVITY, DIELECTRIC FUNCTION, AND POLARITON DISPERSION

Figure 2 presents our results for the far-infrared reflectivity of single-crystal anatase, for $E\|c$ and $E\perp c$. (The frequency or photon-energy scale used throughout this paper is in terms of wave number, $\overline{\nu}=\lambda^{-1}$.) The $E\|c$ results, obtained for a surface containing the c axis, required the use of a polarizer which cut off below 200 cm^{-1}. The incident light was polarized perpendicular to the plane of incidence. The $E\perp c$ results, obtained for a surface normal to the c axis, required no polarizer and extended down to 50 cm^{-1}. (The 50–100 cm^{-1} range, not shown in Fig. 2, contained no discernible structure.)

The theoretical curves included in Fig. 2 are based on the factorized form of the dielectric function:[2,7–9]

$$\varepsilon(\nu)=\varepsilon_1(\nu)-i\varepsilon_2(\nu)=\varepsilon_\infty\prod_n \frac{\nu_{\mathrm{LO}n}^2-\nu^2+i\gamma_{\mathrm{LO}n}\nu}{\nu_{\mathrm{TO}n}^2-\nu^2+i\gamma_{\mathrm{TO}n}\nu}. \quad (1)$$

The factorized form is more elegant than the classical-oscillator form,[7,8] and it is especially appropriate to highly ionic crystals (such as anatase) which have large TO-LO splittings. When ν_{LO} is much larger than ν_{TO}, a single damping parameter γ (as is used in oscillator analysis) is inadequate and the factorized-form analysis is more successful.[2,9] We carried out both oscillator and factorized-form analyses of the data shown in Fig. 2. Both methods give good fits (and essentially identical results for ν_{TO} and ν_{LO}) for $E\|c$. But for $E\perp c$, only the factorized form gives a good fit to the measured reflectivity spectrum.

Table I lists the TO and LO frequencies corresponding to the fitted curves shown in Fig. 2. Also included in the table are the corresponding damping parameters and two sets of published calculations for the TO and LO frequencies using rigid-ion[10] and GF-matrix[4] models. The calculations tend to overestimate the vibrational frequencies and underestimate the TO-LO splittings (oscillator strengths).

In the $E\perp c$ results of Fig. 2, it can be seen that the measured reflectivity shows a small dip (relative to the theoretical curve) near 750 cm^{-1}. It is not an accident that this dip occurs near the LO frequency for the other ($E\|c$) polariza-

TABLE I. TO and LO phonon frequencies of anatase TiO_2.

		Dielectric function fit to $R(\overline{\nu})$		Published calculations	
Mode		Frequency $\overline{\nu}$ (cm^{-1})	Damping γ (cm^{-1})	Rigid ion (Ref. 12) $\overline{\nu}$ (cm^{-1})	GF matrix (Ref. 4) $\overline{\nu}$ (cm^{-1})
$E\|c$ axis	TO	367	68	566	654
(A_{2u})	LO	755	79	844	
$E\perp c$ axis	TO	262	36	329	169
(E_u)	LO	366	4.1	428	
	TO	435	32	644	643
	LO	876	33	855	

$\varepsilon_\infty(E\|c)=5.41$ $\varepsilon_0(E\|c)=22.7$
$\varepsilon_\infty(E\perp c)=5.82$ $\varepsilon_0(E\perp c)=45.1$

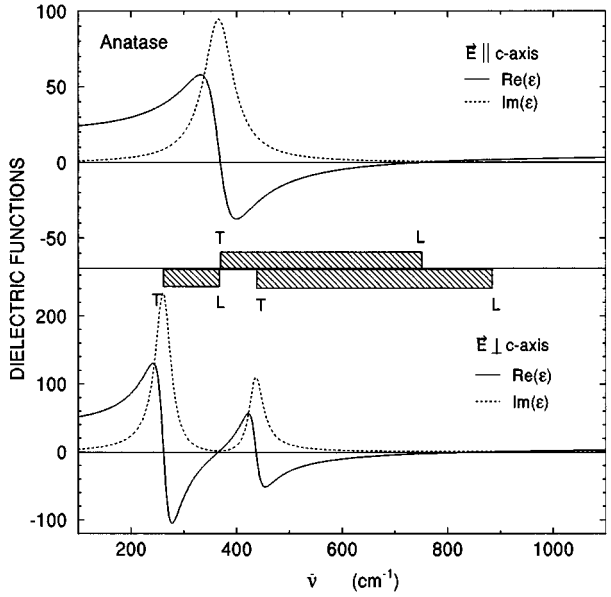

FIG. 3. The dielectric functions of anatase TiO_2. These curves correspond to the fits obtained with the factorized form of the dielectric function. The shaded bars highlight the TO-LO splittings.

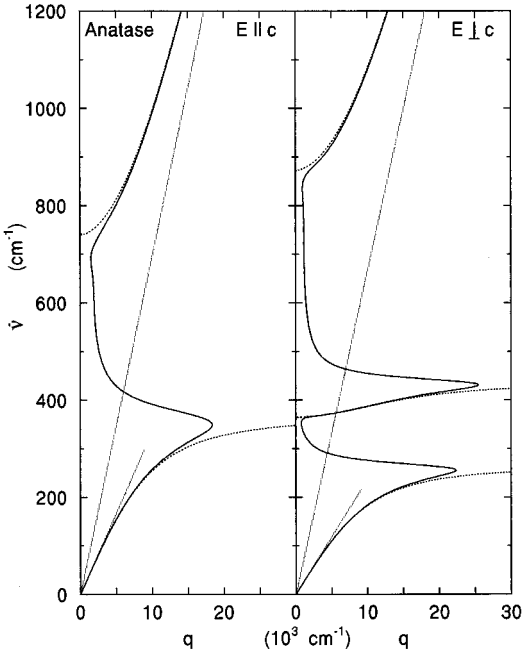

FIG. 4. Polariton dispersion curves for anatase TiO_2. The solid curves correspond to the experimental parameters of Table I. The dashed curves result from setting the damping parameters equal to zero. The light lines show the asymptotic slopes, which are inversely proportional to the optical refractive index (long line) and static refractive index (short line).

tion. The dip is a consequence of the experimental geometry, the 11° deviation from normal incidence. The effects of off-normal incidence, for optically uniaxial crystals (two independent polarizations, $E\|c$ and $E\perp c$), have been experimentally established and theoretically analyzed by several authors.[11–13]

With the c axis normal to the surface and the incident beam polarized in the plane of incidence, an $E\|c$ LO mode that is situated in frequency between a pair of $E\perp c$ TO and LO modes will produce a dip in the $E\perp c$ high-reflectivity plateau at the position of the $E\|c$ LO mode.[11] Our measurements for $E\perp c$ were obtained on a normal-to-c surface using unpolarized light, which includes a component contributing such ''leakage'' (structure arising from the unintended $E\|c$ infrared response function). This off-normal-incidence leakage effect accounts for the 750-cm^{-1} dip observed in the measured $E\perp c$ spectrum of Fig. 2.

There is a similar off-normal-incidence leakage effect for the $E\|c$ reflectivity when it is measured with the c axis and the light polarization in the plane of incidence.[12,13] Since our measurements were carried out with the c axis and the light polarization perpendicular to the plane of incidence, this effect is absent here. The structure in the $E\|c$ spectrum near 640 cm^{-1} is not attributable to off-normal incidence. There is a Raman-active mode in anatase at 639 cm^{-1} (Ref. 4), but anatase is centrosymmetric so that Raman-active modes are infrared-forbidden and do not contribute to the infrared response. (Such modes are not turned on, in infrared reflectivity, by oblique incidence.) The weak 640-cm^{-1} feature in Fig. 2, if real, remains unexplained.

The ε_∞ values in Table I, for frequencies well above the lattice-fundamental regime, correspond to ε's at frequencies below the electronic interband regime. Using $\varepsilon=n^2$ where n is the refractive index, our ε_∞ values correspond to refractive indices of 2.33 ($E\|c$) and 2.41 ($E\perp c$). Reported values of n in the visible region are[14] 2.49 ($E\|c$) and 2.56 ($E\perp c$), indicating that our n values are about 6% low. This does not affect our results for the TO and LO frequencies, which are predominantly determined by the shape of the reflectivity spectrum. We estimate the probable error in our frequency values to be no more than ± 3 cm^{-1} for the TO and $E\|c$ LO frequencies, and ± 5 cm^{-1} for the $E\perp c$ LO frequencies.

From the experimental values given in Table I and the $\varepsilon(\nu)$ expression of Eq. (1), it is straightforward to determine the following spectroscopic quantities in the far infrared: the real and imaginary parts of the dielectric function ε, the real and imaginary parts of the complex refractive index n^c, the optical absorption coefficient, and the polariton dispersion curves $\nu(q_1)$, where q_1 is the real part of the complex propagation vector describing the coupled photon-phonon wave in the crystal.[15] We limit our discussion of spectroscopic quantities to the dielectric function and the polariton dispersion.

Figure 3 shows the results derived for the $E\|c$ and $E\perp c$ dielectric functions for anatase, in the far infrared. The shaded bars highlight the TO-LO splittings, which are large.

Polariton dispersion curves are shown in Fig. 4. The steps from $\varepsilon(\overline{\nu})$ to $\overline{\nu}(q_1)$ are[15] $n^c(\overline{\nu})=\sqrt{\varepsilon(\overline{\nu})}$, $q^c(\overline{\nu})=2\pi\overline{\nu}n^c(\overline{\nu})$, $q_1(\overline{\nu})=\mathrm{Re}[q^c(\overline{\nu})]$. The solid curves correspond to the experimental factorized-form parameters of Table I. The dashed curves results from setting the damping parameters equal to zero; they display the classical coupled-wave from with $q=0$ intercepts at LO frequencies and $q\to\infty$ asymptotes at TO frequencies.[16] The light lines show the asymptotic slopes, which are inversely proportional to the optical refractive index (long line) and static refractive index (short line).

V. EFFECTIVE CHARGES

The vibrational eigenvector of the lone A_{2u} optical mode in anatase is fully determined by symmetry: the atomic displacements x_{Ti} and x_{O} are parallel to the c axis and $(x_{\mathrm{Ti}}/x_{\mathrm{O}})=-0.67$. [The mass ratio $(m_{\mathrm{Ti}}/m_{\mathrm{O}})$ is 2.994.] This presents us with an opportunity to estimate effective charges, using the approach of Kurosawa.[7] Since TiO_2 is highly ionic, we assign static charges (e^*_{Ti} and e^*_{O}) to the ions and assume these charges move with the ions. This is a rigid-ion model, with dynamic charge[17] neglected. The $E\|c$ dielectric function can then be written[7]

$$\varepsilon(\omega)=\varepsilon_\infty+4\pi V^{-1}\left[\sum_i e_i^* x_i\right]^2\left[\sum_i m_i x_i^2\right]^{-1}(\omega_{\mathrm{TO}}^2-\omega^2)^{-1}, \tag{2}$$

where $\omega=2\pi\nu$ is the angular frequency. V is the volume per TiO_2 unit, x_i is the displacement of ion i, e_i^* is the ion's charge, and m_i is its mass. From Eq. (2) and $(x_{\mathrm{Ti}}/x_{\mathrm{O}})=-0.67$ and $(e^*_{\mathrm{Ti}}/e^*_{\mathrm{O}})=-2$ (crystal neutrality) and $(m_{\mathrm{Ti}}/m_{\mathrm{O}})=2.994$, it follows that

$$\varepsilon_0-\varepsilon_\infty=4\pi V^{-1}(e^*_{\mathrm{O}})^2(0.30m_{\mathrm{O}})^{-1}\omega_{\mathrm{TO}}^{-2}. \tag{3}$$

Every quantity in Eq. (3) is known except for e^*_{O}, which is thus determined: $e^*_{\mathrm{O}}=-2.8e$, where e is the magnitude of the electron charge and the negative sign is chosen for the oxygen ion. The result is reasonable, but somewhat large; we do not expect the oxygen ion to be more highly charged than O^{--}, and any contribution from dynamic charge would be expected to reduce the size of the observed effective charge.[18] Szigeti's introduction of the local-field correction in the case of a cubic crystal[19] reduces the effective charge by the factor $3/(\varepsilon_\infty+2)$. TiO_2 is not cubic, but the TO-LO splittings of Fig. 3 are larger than the anisotropy shifts so neglecting anisotropy may not be a terrible approximation. Doing this yields a Szigeti effective charge, for the oxygen ion, of $-1.1e$.

VI. SUMMARY

Single crystals of anatase, grown by transport reactions, were studied by far-infrared reflectivity. Clean polarization-dependent spectra were observed (Fig. 2), and the results were analyzed to yield the dielectric dispersion properties in the lattice fundamentals regime (Figs. 3 and 4). The TO (and LO) frequencies of the zone-center phonons were determined to be (in units of cm^{-1}): 367(755) for the A_{2u} mode; 262(366) and 435(876) for the E_u modes. The large TO-LO splitting was analyzed in terms of effective charges for the A_{2u} mode, whose vibrational eigenvector is symmetry determined.

ACKNOWLEDGMENTS

We are grateful to A. Gaynor and R. M. Davis of the Chemical Engineering Department at Virginia Tech for many discussions about titania, to B. Kutz of the Department of Geological Sciences for her help in orienting, cutting, and polishing the anatase crystals, and to G. Margaritondo of EPFL for his support and encouragement. Work at EPFL was supported in part by the Fonds Nationale Suisse de la Recherche Scientifique.

*Present address: Sienna Biotech, Inc., Columbia, MD.

[1] W. G. Spitzer, R. C. Miller, D. A. Kleinman, and L. E. Howarth, Phys. Rev. **126**, 1710 (1962).
[2] F. Gervais and B. Piriou, J. Phys. C **7**, 2374 (1974).
[3] J. G. Traylor, H. G. Smith, R. M. Nicklow, and M. K. Wilkinson, Phys. Rev. B **3**, 3457 (1971).
[4] T. Ohsaka, F. Izumi, and Y. Fujiki, J. Raman Spectrosc. **7**, 321 (1978).
[5] H. Tang, F. Levy, H. Berger, and P. E. Schmid, Phys. Rev. B **52**, 7771 (1995).
[6] H. Berger, H. Tang, and F. Levy, J. Crystal Growth **130**, 108 (1993).
[7] T. Kurosawa, J. Phys. Soc. Jpn. **16**, 1298 (1961). Setting $\nu=0$ in the factorized form yields the Lyddane-Sachs-Teller relation.
[8] D. W. Berreman and F. C. Unterwald, Phys. Rev. **174**, 791 (1968).
[9] F. Gervais and B. Piriou, Phys. Rev. B **10**, 1642 (1974); J. F. Baumard and F. Gervais, *ibid.* **15**, 2316 (1977).
[10] N. Krishnamurthy and T. M. Haridasan, Indian J. Pure Appl. Phys. **17**, 67 (1979).
[11] A. S. Barker and M. Ilegems, Phys. Rev. B **7**, 743 (1973).
[12] J. L. Duarte, J. A. Sanjurjo, and R. S. Katiyar, Phys. Rev. B **36**, 3368 (1987).
[13] A. Goullet, J. Camassel, L. Martin, J. Pascual, and E. Philippot, Phys. Rev. B. **40**, 5750 (1989).
[14] *Handbook of Chemistry and Physics*, 68th ed. (CRC Press, Boca Raton, 1987), p. B-193.
[15] R. Zallen, G. Lucovsky, W. Taylor, A. Pinczuk, and E. Burstein, Phys. Rev. B **1**, 4058 (1970); R. Zallen, M. L. Slade, and A. T. Ward, *ibid.* **3**, 4257 (1971).
[16] K. Huang, Proc. R. Soc. (London) **A208**, 352 (1951).
[17] W. Cochran, Nature (London) **191**, 60 (1961); E. Burstein, M. H. Brodsky, and G. Lucovsky, Int. J. Quantum Chem. **15**, 759 (1967); R. Zallen, R. M. Martin, and V. Natoli, Phys. Rev. B **49**, 7032 (1994).
[18] B. G. Dick and A. W. Overhauser, Phys. Rev. **112**, 90 (1958); R. Zallen and G. Lucovsky, in *Selenium*, edited by R. A. Zingaro and W. C. Cooper (Van Nostrand Reinhold, New York, 1976), p. 148.
[19] B. Szigeti, Trans. Faraday Soc. **45**, 155 (1949).